THE JOURNAL OF BIOLOGICAL CHEMISTRY VOL. 291, NO. 46, pp. 24121–24132, November 11, 2016

Quantitative Proteomics of the SMAD (Suppressor of Mothers against Decapentaplegic) Transcription Factor Family Identifies Importin 5 as a Bone Morphogenic Protein Receptor SMAD-specific Importin*[S]

Received for publication, July 15, 2016, and in revised form, October 3, 2016 Published, JBC Papers in Press, October 4, 2016, DOI 10.1074/jbc.M116.748582

Roy Baas, Ayestha Sijm, Hetty A. A. M. van Teeffelen, Robert van Es, Harmjan R. Vos, and H. Th. Marc Timmers[1]

From the Departments of Molecular Cancer Research and Stem Cells, Regenerative Medicine Center, Center for Molecular Medicine, University Medical Center Utrecht, Uppsalalaan 8, 3584 CT Utrecht, The Netherlands

Edited by Xiao-Fan Wang

Gene-specific transcription factors (GSTFs) control gene transcription by DNA binding and specific protein complex recruitment, which regulates promoter accessibility for transcription initiation by RNA polymerase II. Mutations in the GSTFs *Suppressor of Mothers Against Decapentaplegic 2* (*SMAD2*) and *SMAD4* are frequently associated with colon and rectal carcinomas. These proteins play an important role in bone morphogenic protein (BMP) and transforming growth factor β (TGF-β) signaling pathways controlling cell fate and proliferation. To study the protein interactome of the SMAD protein family we generated a quantitative proteomics pipeline that allows for inducible expression of GFP-tagged SMAD proteins followed by affinity purification and quantitative mass spectrometry analysis. Data are available via ProteomeXchange with identifier PXD004529. The nuclear importin IPO5 was identified as a novel interacting protein of SMAD1. Overexpression of IPO5 in various cell lines specifically increases nuclear localization of BMP receptor-activated SMADs (R-SMADs) confirming a functional relationship between IPO5 and BMP but not TGF-β R-SMADs. Finally, we provide evidence that variation in length of the lysine stretch of the nuclear localization sequence is a determinant for importin specificity.

Transcription regulation is a tightly controlled process that is influenced by the binding of gene-specific transcription factors (GSTFs)[2] to specific DNA elements (1). These GSTF families are highly heterogeneous, spanning several hundreds of proteins like the C_2H_2-type zinc fingers (2) to the eight members of the SMAD protein family. Binding of GSTFs to DNA elements mediates recruitment of multisubunit co-activator complexes like SET/MLL, Mediator, TFIID, or the BAF remodeler, each of which can specifically affect the chromatin microenvironment resulting in alteration of gene transcriptional states. Cancer genome-wide association studies have shown that GSTFs and chromatin-associated proteins are often mutated in various solid tumors types (3–5). In particular, mutations in SMAD2 and SMAD4 have been frequently associated with colon and rectal carcinomas (5.7 and 9.8%, respectively) (3). The eight SMAD family members can be divided into the R-SMADs (SMAD1/2/3/5/9), I-SMADs (SMAD6/7), and Co-SMAD (SMAD4) (Fig. 1*A*). R-SMADs can additionally be subdivided into BMP (SMAD1/5/9) and TGF-β (SMAD2/3) subclasses depending on the ligand activating.

SMAD signaling starts with the activation of the anaplastic lymphoma kinase type II receptors by the binding of the BMP or TGF-β cytokines. Activation of type II receptors recruits and phosphorylates anaplastic lymphoma kinase type I receptors, which in turn activate the R-SMADs by phosphorylating the SS*X*S residues in the C-terminal domain (6–8). In basal conditions the SMADs shuttle constantly between the cytoplasm and the nucleus (9) via interaction with the nucleoporins (10). After receptor-mediated R-SMAD activation, an import protein is required for their nuclear translocation. The activated R-SMADs recruit SMAD4 and the complex is transported to the nucleus via different import proteins like IPO7 and IPO8 (11). These importins recognize a conserved stretch of charged lysine residues that acts as a nuclear localization signal (NLS). An NLS is present in the MAD homology 1 (MH1) domain of the R-SMADs, but differs in sequence in the Co-SMAD and I-SMADs (9, 12, 13). Gene activation by SMADs also induces a negative feedback loop through induced expression of I-SMAD target genes SMAD6 and SMAD7, which negatively affect SMAD signaling (14–17).

To study the SMAD GSTF protein family in a comprehensive manner we generated a quantitative proteomics pipeline for human cells. Using this method we identified IPO5 as a novel SMAD1 interactor. Overexpression of IPO5 increases nuclear localization of BMP but not TGF-β R-SMADs, which suggested a functional relationship between BMP signaling and IPO5. Mutation experiments extending the lysine stretch of the NLS of SMAD3 shows that the length of the lysine stretch is involved in differentiating IPO5 and IPO7 as importins for the BMP and TGF-β subgroup of SMAD transcription factors.

* This work was supported by NWO-Life Sciences Grant 821.02.012 (to H. Th. M. T.). The authors declare that they have no conflict of interest with the contents of this article.

[S] This article contains supplemental Figs. S1–S4 and Table S1.

[1] To whom correspondence should be addressed. Tel.: 31-88-756-8981; E-mail: H.T.M.Timmers@umcutrecht.nl.

[2] The abbreviations used are: GSTF, gene-specific transcription factors; SMAD, suppressor of mothers against decapentaplegic; BMP, bone morphogenic protein; R-SMAD, receptor-activated SMAD; NLS, nuclear localization signal; MH1, MAD homology 1; TBP, TATA-binding protein; N/C, nuclear over cytoplasmic; FRT, Flp recombination target; qRT, quantitative RT.

Results

GFP-SMAD Cell Line Generation—To study the interactome of the human SMAD proteins, stable doxycycline-inducible HeLa cell lines containing GFP-SMAD fusion proteins or GFP without fusion partner as control were generated using the Flp-In T-Rex system (supplemental Fig. S1). To characterize expression of the GFP fusion proteins, a doxycycline induction time series was performed. Immunoblot shows maximal protein expression after 16 h with no further increase at 20- or 24-h induction time points (Fig. 1*B*). SMAD protein activity is regulated via post-translational modifications affecting protein localization and functional SMADs are expected to shuttle between the cytoplasm and nucleus. Indeed, confocal microscopy shows that all GFP-SMADs can be detected both in the cytoplasm and nucleus (Fig. 2) suggesting that localization of the fusion proteins is not impaired by the N-terminal GFP tag. Subsequently, we tested SMAD activation evaluating the phosphorylation status of SMAD2 upon TGF-β stimulation using phosphor-specific antibodies. Phosphorylated GFP-SMAD2 and endogenous SMAD2 was detected in treated and untreated conditions suggesting the TGF-β pathway is (partially) active under normal HeLa cell culture conditions (Fig. 3*A*). To confirm this observation, the SB431542 inhibitor of TGF-β signaling (18) was added in various concentrations to the HeLa GFP-SMAD2 cell line 1 h prior to harvesting (Fig. 3*B*). A decrease in phosphorylation of both GFP-SMAD2 and endogenous SMAD2 was observed compared with untreated control samples confirming active TGF-β signaling under normal cell culture conditions. To determine whether BMP signaling is also activated under normal HeLa cell culture conditions, we treated GFP-SMAD5 cells with the BMP signaling inhibitor LDN193189. Again, phosphorylation levels of endogenous and GFP-SMAD5 were reduced compared with control conditions (Fig. 3*C*), suggesting active BMP signaling. Overall, partially active TGF-β and BMP signaling pathways are consistent with detection of GFP-SMAD proteins both in the cytoplasm and nucleus (Fig. 2). These data show that we generated stable inducible HeLa cell lines expressing functional GFP-SMAD proteins.

SMAD Interactome Identification Using Mass Spectrometry—Localization of GFP-SMAD proteins to both the cytoplasm and nucleus suggests different pools of proteins with different biological activity and/or interaction partners. To systematically study these different SMAD pools we prepared cytoplasmic and nuclear extracts from the GFP-SMAD cell lines after 16–20 h of doxycycline induction (Fig. 4*A*). Immunoblot analysis of cytoplasmic and nuclear fractions confirmed the GFP fluorescence results of Fig. 2. Blots were developed with antibodies against the nuclear TATA-binding protein (TBP) or cytoplasmic tubulin as controls. We found that GFP-SMAD1, -SMAD5, and -SMAD7 are expressed to lower levels as the other GFP-SMADs. To determine the interactome of SMAD proteins cytoplasmic and nuclear extracts were subjected to GFP affinity purification using nanobeads (Fig. 4*B*). All purifications were performed in triplicate and measured by MS/MS analysis using a Velos mass spectrometer. In total, 108 affinity purifications were performed and all data files were

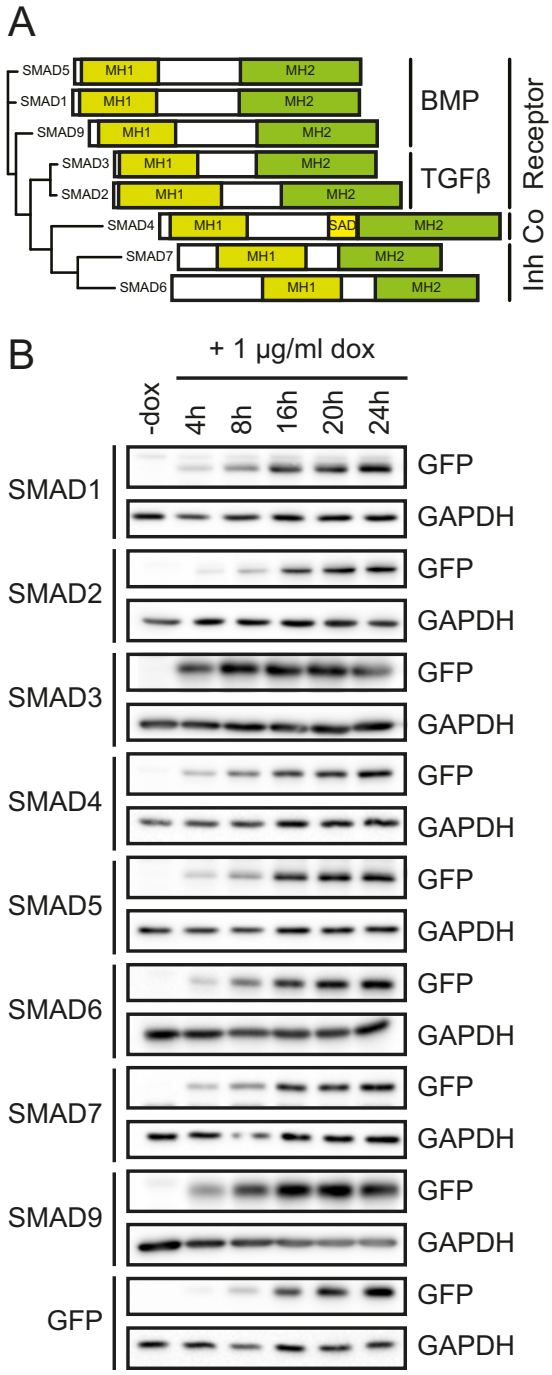

FIGURE 1. **Generation of GFP-SMAD cell lines.** *A,* SMAD protein phylogeny. Clustering analysis and systemic representation of SMAD proteins with the indicated domains (MH1, MH2, and SAD). SMAD categorization is indicated on the *right*. *B,* SMAD cell line time series after doxycycline induction was analyzed on immunoblot. HeLa cell lines were induced with 1 μg/ml of doxycycline for 4, 8, 16, 20, or 24 h prior to harvesting or harvested without induction. Blots were probed using GFP or GAPDH antibodies.

simultaneously analyzed using MaxQuant. Correlation plots show very good reproducibility between all samples (supplemental Fig. S2). A clear correlation is observed between samples within the same cell line for the extracts (cytoplasmic *versus* nucleus), although no clear correlation is observed between extracts from separate GFP-SMAD cell lines.

The data were visualized using scatterplots, which were generated with the median data obtained for each triplicate set.

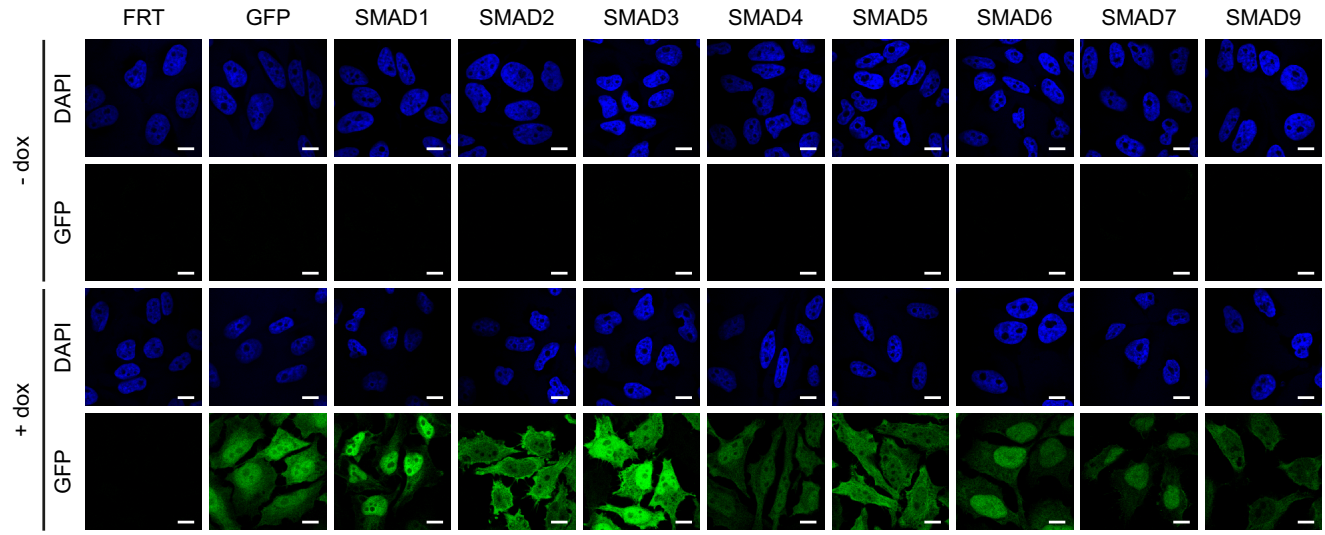

FIGURE 2. **Analysis of GFP-SMAD expression.** Doxycycline (*dox*) induction test for confocal microscopy shows GFP fusion protein localization. HeLa cell lines were seeded on coverslips and induced with 1 μg/ml of doxycycline for 16 h prior to fixing and analyzed using confocal microscopy.

Hereby, the affinity-purified samples were plotted as x values against its corresponding control situation as the y values. When using this data representation a protein cloud is expected on the diagonal representing proteins that nonspecifically bind to the beads (Figs. 5 and 6). Proteins that bind to the GFP-tagged bait protein will be more abundant in the affinity purification with the GFP-binding beads and therefore, they will be shifted from the diagonal toward the x axis. In certain situations, for example, when a protein is only expressed in a low amount, proteins will only be identified when enriched using the GFP-binder beads but not the control beads. To include these cases a constant value was imputed for missing data points to plot values that only contain a value for one bead type. When the results are plotted the data forms a horizontal line for proteins identified only on GFP-binding beads and a vertical line for proteins only identified on control beads. Proteins present on the horizontal line are therefore also regarded as enriched, but the fold-enrichment cannot be calculated.

As validation of the mass spectrometry data from the nuclear fraction, we examined SMAD enrichment in different SMAD baits (Fig. 5). As expected, the SMAD2/3/4 proteins interact with each other in the nucleus. Furthermore, the TGF-β inhibitory proteins SKI and SKIL are present in SMAD2/3/4 affinity purifications. These two proteins are known direct interactors of the SMAD2/3/4 complex (19, 20). In addition and as expected, we identified the R-SMAD inhibitor LEMD3 (MAN1) (21, 22) as a SMAD3 interactor. Interestingly, LEMD3 is not enriched in SMAD4 affinity purifications. This indicates that LEMD3 and SMAD4 are mutually exclusive binders for SMAD2/3 and fit the current view that LEMD3 is a repressor of R-SMAD activation (21, 22). LEMD3 is not enriched in SMAD1/2/5, whereas this interaction has been described before (22). This could be a HeLa-specific or a transcriptional status effect. A new interaction of LEMD3 with SMAD9 is also identified and complements the current view on LEMD3 as a repressor of R-SMAD activation. Next, several complexes that have different functions in the nucleus were visualized for enrichment in the nuclear fractions (Fig. 5 and supplemental Table S1). Enrichment for several of the TFIID, SET1/MLL, and Mediator subunits were observed in SMAD1 and SMAD2, whereas no enrichment was observed in other SMADs or the GFP control cell line. The TFIID, SET1/MLL, and Mediator complexes are known for their activating role in pol II-mediated transcription. As a control we examined the pol III transcription factor TFIIIC and found that it was not enriched in any SMAD cell line, nor was the BAF chromatin regulatory complex. This suggests that SMAD1 and SMAD2 are employing specific transcription co-activator complexes to stimulate pol II-mediated transcription.

To examine the quantitative proteomics results for the cytoplasmic fraction the data were also represented as scatterplots. Apart from the expected background distribution a second protein distribution, absent in the nuclear fraction was observed (supplemental Fig. S3*A*). Gene ontology term analysis shows enrichment for unfolded protein binding and protein biosynthesis (supplemental Fig. S3*B*). Possibly the interactors were identified due to incomplete synthesis of the GFP-SMAD proteins, although no discrete partial GFP-SMAD proteins are observed by immunoblotting (Fig. 4*A*). Alternatively, the GFP-SMAD fusion protein might be incorrectly folded. It is important to note that this secondary distribution is not observed in the affinity purifications of the GFP control samples from the cytoplasmic fraction.

SMAD proteins require transport proteins to shuttle between the cytoplasm and nucleus. To investigate which transport proteins associate with the different SMADs all transport proteins were identified in the cytoplasmic fraction plots. For the different SMADs various transport proteins were found enriched, whereas in the GFP control cell line most transport proteins were identified in the background diagonal. SMAD4, which needs an R-SMAD as partner to translocate to the nucleus, does not contain any enriched transport proteins. SMAD1 shows enrichment for several transport proteins like the previously reported IPO7 (11), but also displays a strong enrichment of IPO5 (Fig. 6).

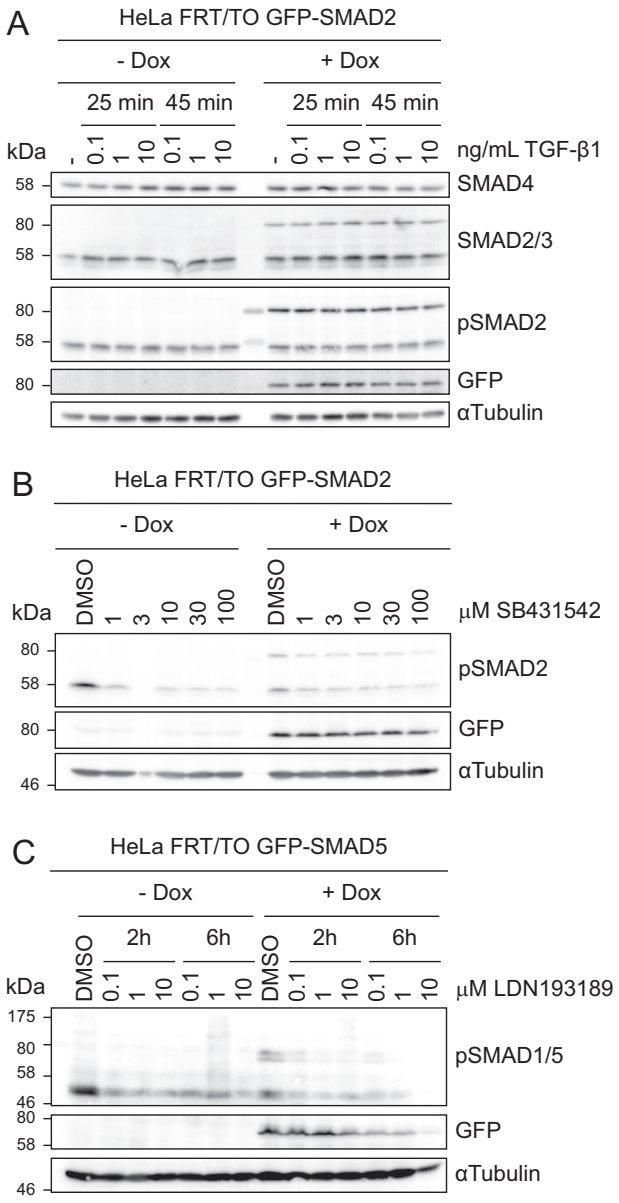

FIGURE 3. **GFP-SMAD fusion constructs are responsive to phosphorylation.** *A,* TGF-β stimulation titration on HeLa GFP-SMAD2 expressing cells on two time points. Cells were seeded and induced with doxycycline for 16 h where indicated. Cells were induced with 0.1, 1, or 10 ng/ml TGF-β for 25 or 45 min prior to harvesting. Samples were analyzed on immunoblot using SMAD4, SMAD2/3, phospho-SMAD2, GFP, and α-Tubulin antibodies. *B,* SB431542 inhibitor titration on HeLa GFP-SMAD2 expressing cells. Cells were seeded and induced with doxycycline (Dox) for 16 h where indicated. Inhibitor was added with 1, 3, 10, 30, or 100 μM 60 min prior to harvesting. Samples were analyzed on immunoblot using phospho-SMAD2, GFP, and α-Tubulin antibodies. *C,* LDN193189 inhibitor titration on HeLa GFP-SMAD5 expressing cells on two time points. Cells were seeded and induced with doxycycline for 16 h where indicated. Inhibitor was added with 0.1, 1, or 10 μM 60 min prior to harvesting. Samples were analyzed on immunoblot using phospho-SMAD1/5, GFP, and α-Tubulin antibodies.

Confirmation of Importin 5 as a Novel Interactor of SMAD1—Control of subcellular localization is important for the biological function of SMAD proteins. IPO7 overexpression was shown previously to force nuclear translocation of SMAD1/3/4 proteins (11). To investigate the function of IPO5 as a SMAD interactor we coexpressed all GFP-SMAD fusion proteins with IPO5 or IPO7 in human U-2 OS osteosarcoma cells to measure the ratio of nuclear over cytoplasmic (N/C) GFP intensities. As expected, overexpression of IPO7 stimulates nuclear localization of the receptor-activated SMADs 1, 2, 3, 5, and 9 but not the inhibitory SMADs 6 and 7 or the common SMAD4 (Fig. 7). Strikingly, overexpression of IPO5 forced nuclear localization of BMP subclass R-SMADs 1, 5, and 9 but not TGF-β subclass R-SMADs 2 and 3 suggesting IPO5 subclass specificity. IPO5- and IPO7-dependent nuclear localization was confirmed for SMAD1 and SMAD3 in the human breast adenocarcinoma cell line MCF7 (supplemental Fig. S4). Knockdown of IPO5 or IPO7 using siRNA in HeLa GFP-SMAD stable cell lines gave inconclusive results (data not shown) except for SMAD1 and -3, which accumulated reproducibly in the cytoplasm (Fig. 8). Compared with IPO7, knockdown of IPO5 has a small effect on GFP-SMAD3. IPO5 has been shown to interact with the RanBP1 and RanBP2 proteins (23, 24). Knockdown of RanBP1 or RanBP2 using siRNAs was performed in HeLa cells expressing GFP-SMAD1 or GFP-SMAD3 to investigate their subcellular distribution. We found N/C ratios of these SMAD proteins are reduced significantly upon RanBP2 but not RanBP1 knockdown (Fig. 9, *A–D*). Because IPO5 and IPO7 facilitate nuclear localization of BMP R-SMAD proteins, expression of IPO5 and IPO7 were examined in context of BMP activation. Both IPO5 and IPO7 levels remained constant upon BMP stimulation or inhibition in U-2 OS cells. As expected pSMAD1/5 levels are responsive to activation and repression of BMP signaling (Fig. 9*E*). Taken together, the overexpression and knockdown results support involvement of IPO5 in the subcellular distribution of a subset of SMAD proteins.

An Extended NLS Lysine Stretch Is Required for IPO5 Nuclear Import—The NLS of SMAD proteins consists of an N-terminal basic motif and it is localized in the MH1 domain. R-SMADs contain the canonical KKLKK sequence. However, BMP R-SMADs carry a basic stretch extended by two additional lysines (KK) compared with TGF-β R-SMADs (-T) (Fig. 10*A*). To investigate the molecular mechanism by which IPO5 distinguishes between the BMP and TGF-β R-SMADs, the NLS of SMAD3 (SMAD3 wt) was replaced by the NLS containing a long lysine stretch (SMAD3 T45K 45insK). Overexpression of SMAD3 T45K 45insK with IPO5 stimulates nuclear localization, which is not observed in the SMAD3 wt control (Fig. 10*B*). These results suggest that IPO5-mediated nuclear localization is dependent on an extended lysine stretch present in the NLS of the BMP induced R-SMADs.

Discussion

SMAD signaling is involved in many different cellular processes. In this study interactome datasets for all SMAD proteins were generated using affinity purification for HeLa cells followed by mass spectrometry analysis. The nuclear transport protein IPO5 was identified as a novel interactor for BMP-regulated SMAD1 and using confocal microscopy a functional link was shown between IPO5 and the BMP-regulated R-SMADs but not TGF-β-regulated R-SMADs. By extending the NLS lysine stretch in SMAD3 we found SMAD3 nuclear localization sensitive to IPO5, suggesting that the length of the lysine stretch in the NLS is responsible for differentiation between the BMP- and TGF-β-regulated SMADs.

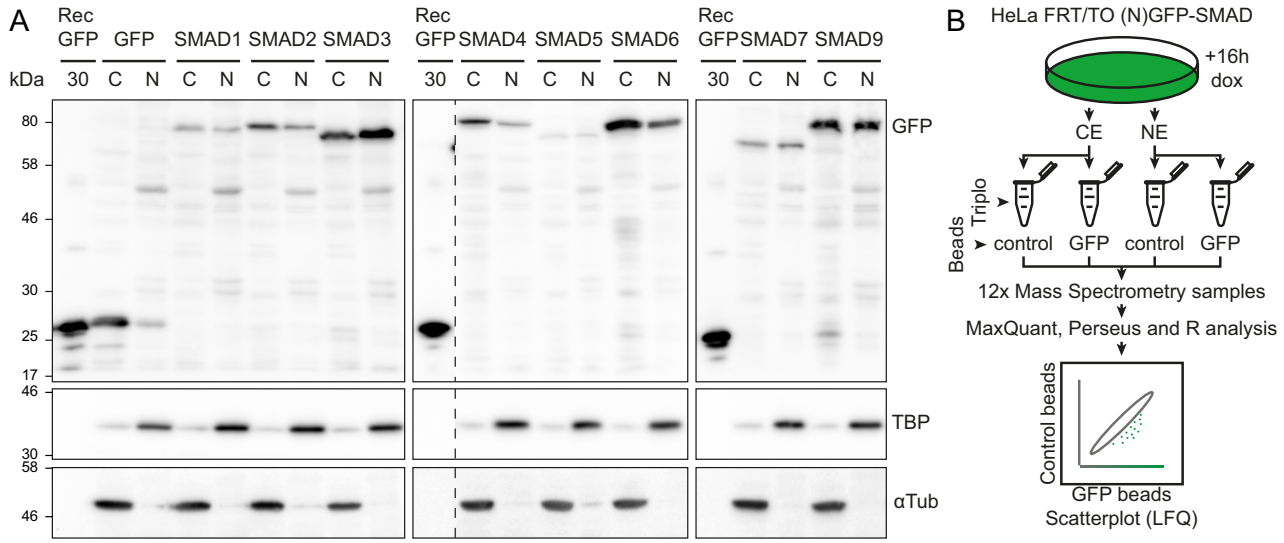

FIGURE 4. **Analysis of nuclear and cytoplasmic extracts and mass spectrometry approach.** *A,* immunoblot containing 50 μg of input protein originating from cytoplasmic and nuclear extracts were analyzes using GFP antibodies. Recombinant GFP (30 ng) was run in parallel for reference. Samples were analyzed using GFP, TBP, and α-Tubulin antibodies. The *dashed line* indicates removal of lanes unrelated to this experiment on the blot. *Rec GFP*, recombinant GFP; *C*, cytoplasmic fraction; *N*, nuclear fraction. *B,* schematic representation of experimental workflow. Cytoplasmic and nuclear extracts were prepared from HeLa GFP fusion protein expressing cells. GFP pulldown or mock pulldown experiments were performed on the extracts in triplicate. Samples were measured by mass spectrometry and raw data were analyzed using MaxQuant, Perseus, and visualized in R.

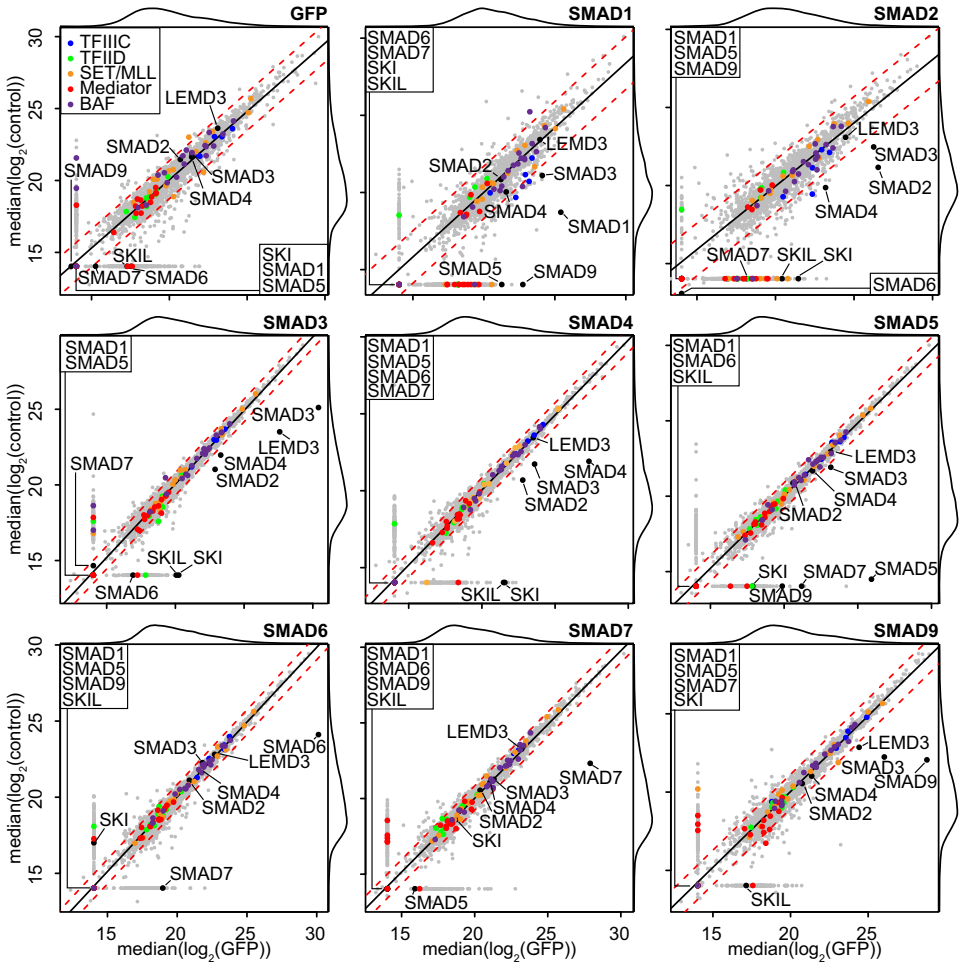

FIGURE 5. **Mass spectrometry analysis for nuclear fractions.** Scatterplot representations for nuclear fraction affinity purifications. GFP affinity purifications (*x* axis) were plotted against control purifications (*y* axis). Subunits from TFIIIC (*blue*), TFIID (*green*), SET/MLL (*orange*), Mediator (*red*), and BAF (*purple*) complexes are highlighted using their respective colors and SMADs, SKI, SKIL, and LEMD3 are indicated. The continuous *black line* and *dotted red lines* represent a linear model based on the data with the respective 95% confidence interval. A distribution of all proteins without an imputed value is indicated in the *top* and *right sides* of the scatterplot.

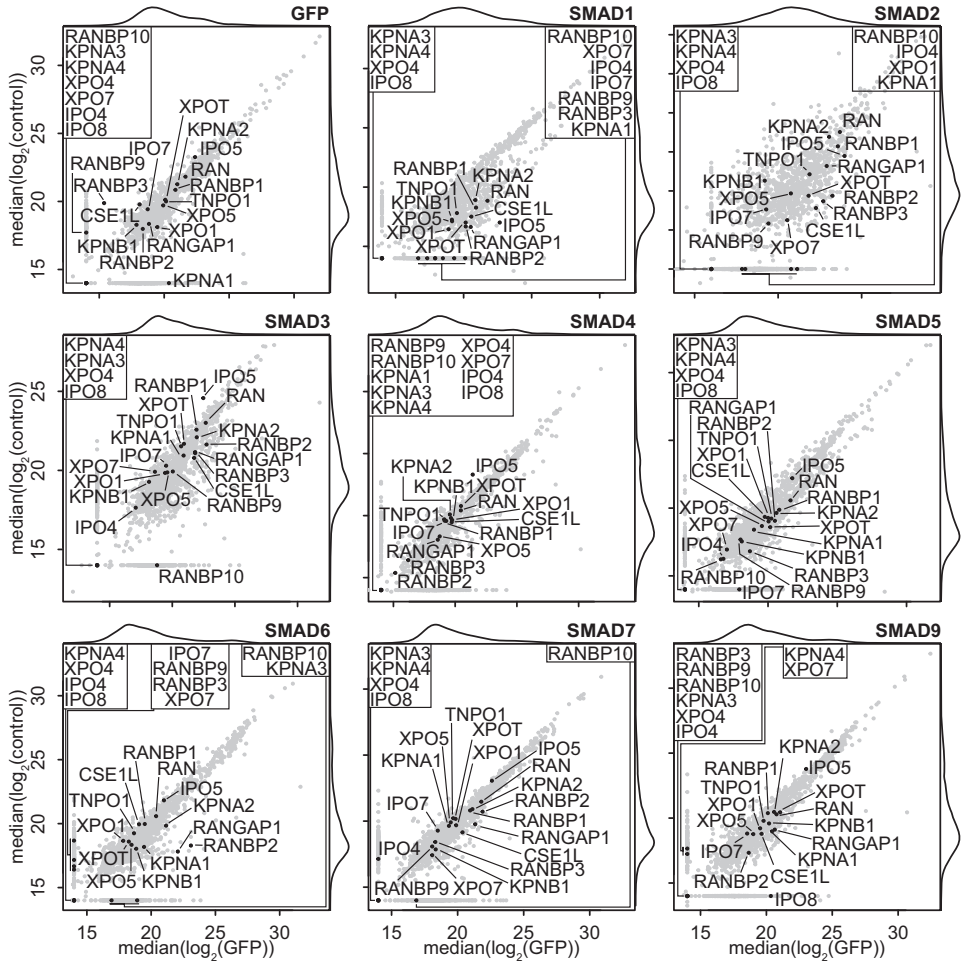

FIGURE 6. **Mass spectrometry analysis for cytoplasmic fractions.** Scatterplot representations for cytoplasmic fraction affinity purifications. GFP affinity purifications (*x* axis) were plotted against control purifications (*y* axis). Identified transport proteins are highlighted. A distribution of all proteins without an imputed value is indicated in the *top* and *right sides* of the scatterplot.

SMAD proteins shuttle continuously between the cytoplasm and nucleus, which is independent of a receptor activation signal (9). The export of SMAD4 is known to be CRM1-mediated, whereas export of R-SMADs is CRM1-independent. Phosphorylation of R-SMAD followed by SMAD4 recruitment causes nuclear accumulation of SMADs, which result in reduced nuclear export. Transcription factors like TAZ (25) have been shown to be responsible for SMAD nuclear accumulation, although the exact mechanism is unknown. In the nucleus, phosphorylation of R-SMAD complexes is gradually reduced causing dissociation of SMAD4 followed by export from the nucleus. This constant SMAD nuclear/cytoplasmic cycling is an important control mechanism for constant monitoring of the receptor activation status. This results in a quick adaptation of nuclear SMAD accumulation, when the signal is present and to reduce to steady state levels when the receptors become inactive. Initially, transport proteins importin α1 and β1 (26) have been connected with SMAD signaling. Later studies implied IPO7 and IPO8 in signal-dependent and -independent transport of SMAD1/3/4 involving NLS found in the MH1 domain. Our results corroborate an important role of IPO7 in subcellular distribution of SMAD1, -2, -3, -5, and -9 (Fig. 7). IPO7 seems to be the major contributor of SMAD nuclear import, whereas the import mediated by IPO5 is restricted. Nuclear import of the R-SMADs by IPO7 does not select for a specific type of R-SMAD (Fig. 7). Systemically testing IPO5 against all SMADs in this study shows selectivity of IPO5 for BMP-activated R-SMADs, which is determined by the length of the lysine stretch of the NLS. Selectivity of the IPO5 protein for the cargo allows for regulation of signaling, thus adding a new player in controlling the subcellular distribution of SMAD proteins.

The SMAD activation pathway is a signaling cascade that gains complexity in regulation over different levels in the cell (14, 27–32). Over 30 different molecules including TGF-β and BMP can be found in the human body that belong to the TGF-β superfamily (33). These molecules can signal to a combination of seven type I and five type II receptors. Because not all of these receptors are present in each cell type this makes TGF-β and BMP signaling very context-dependent. It is important to note that we did not identify any TGF-β or BMP receptor in GFP-SMAD purifications from the cytoplasmic fractions, which could be due to the low efficiency of membrane protein extraction in our procedures.

The N-terminal location of the GFP moiety in the SMAD fusion constructs was chosen to maintain the C-terminal SS*X*S

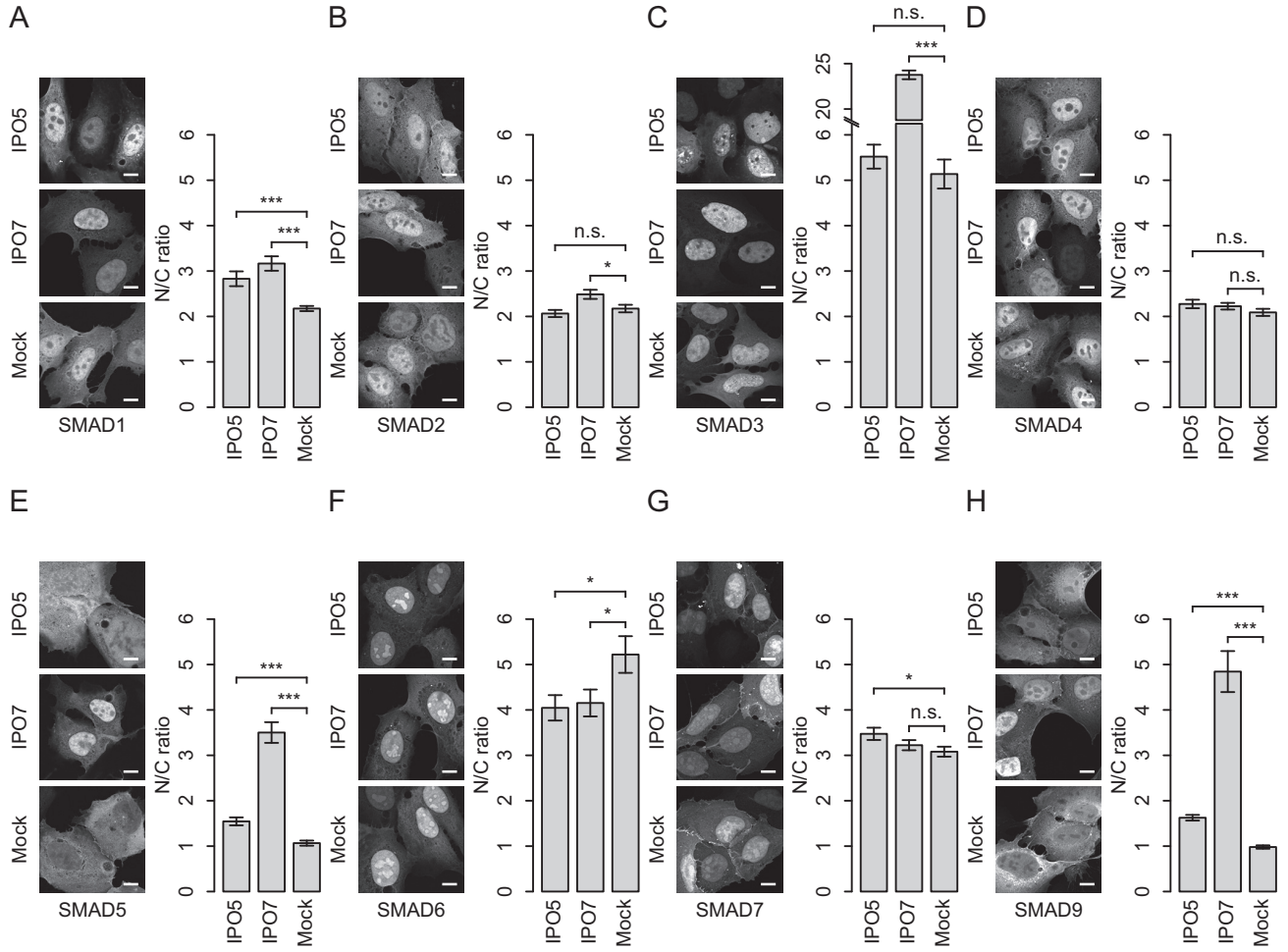

FIGURE 7. **Overexpression of IPO5 stimulates nuclear localization of BMP- but not of TGFβ-activated R-SMADs.** *A–H,* U-2 OS cells were seeded on coverslips and transfected using a combination of GFP-SMADs with FLAG-IPO5, FLAG-IPO7, or mock. Cells were fixed 48 h after transfection and analyzed using confocal microscopy. Nuclear and cytoplasmic intensities were quantified using ImageJ. Shown is combined data of $n = 2$ biological replicates with varying technical replication *n* specified per set. *Bars* represent average nuclear/cytoplasmic (N/C) ratio, *error bars* represent mean ± S.E. Significant differences are indicated for various significance levels (***, $p < 0.001$; **, $0.001 < p < 0.01$; *, $0.01 < p < 0.05$; *n.s.*, not significant). *Scale bar,* 10 μm. *A,* SMAD1 N/C ratios. Technical replication $n = 55, 61$, and 74. *B,* SMAD2 N/C ratios. Technical replication $n = 72, 67$, and 67. *C,* SMAD3 N/C ratios. Technical replication $n = 61, 71$, and 62. *D,* SMAD4 N/C ratios. Technical replication $n = 70, 59$, and 70. *E,* SMAD5 N/C ratios. Technical replication $n = 46, 45$, and 41. *F,* SMAD6 N/C ratios. Technical replication $n = 47, 55$, and 46. *G,* SMAD7 N/C ratios. Technical replication $n = 62, 58$, and 66. *H,* SMAD9 N/C ratios. Technical replication $n = 64, 55$, and 64.

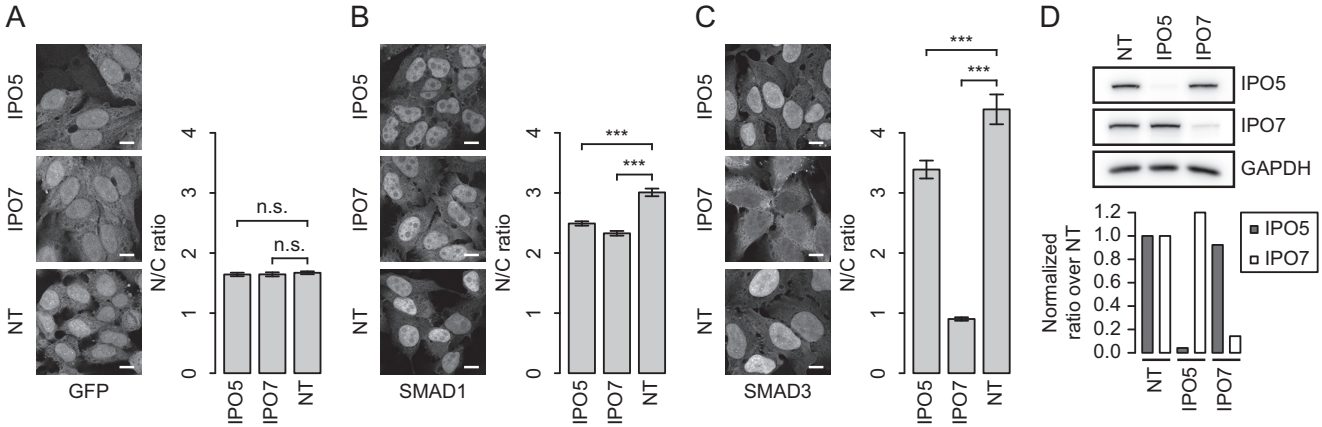

FIGURE 8. **Knockdown of IPO5 reduces nuclear localization of SMAD1.** *A–C,* HeLa cell lines were transfected with siRNA against non-targeting, IPO5 or IPO7. Cells were induced with 1 μg/ml of doxycycline for 16 h prior to fixing and analyzed 72 h after siRNA transfection using confocal microscopy. Nuclear and cytoplasmic GFP intensities were quantified using ImageJ. A representative experiment is shown. *Bars* represent the average N/C ratio, *error bars* represent mean ± S.E. Significant differences are indicated for various significance levels (***, $p < 0.001$; **, $0.001 < p < 0.01$; *, $0.01 < p < 0.05$; *n.s.*, not significant). *Scale bar,* 10 μm. *A,* GFP N/C ratios. Technical replication $n = 63, 62$, and 69. *B,* SMAD1 N/C ratios. Technical replication $n = 70, 80$, and 64. *C,* SMAD3 N/C ratios. Technical replication $n = 57, 59$, and 58. *D,* knockdown efficiency of IPO5 and IPO7 in non-induced HeLa GFP cells. Cells were reverse transfected with siNT, siIPO5, or siIPO7 and collected after 72 h. Samples were analyzed on an immunoblot and bands were quantified in ImageJ. Band intensities were corrected for GAPDH expression and normalized to siNT.

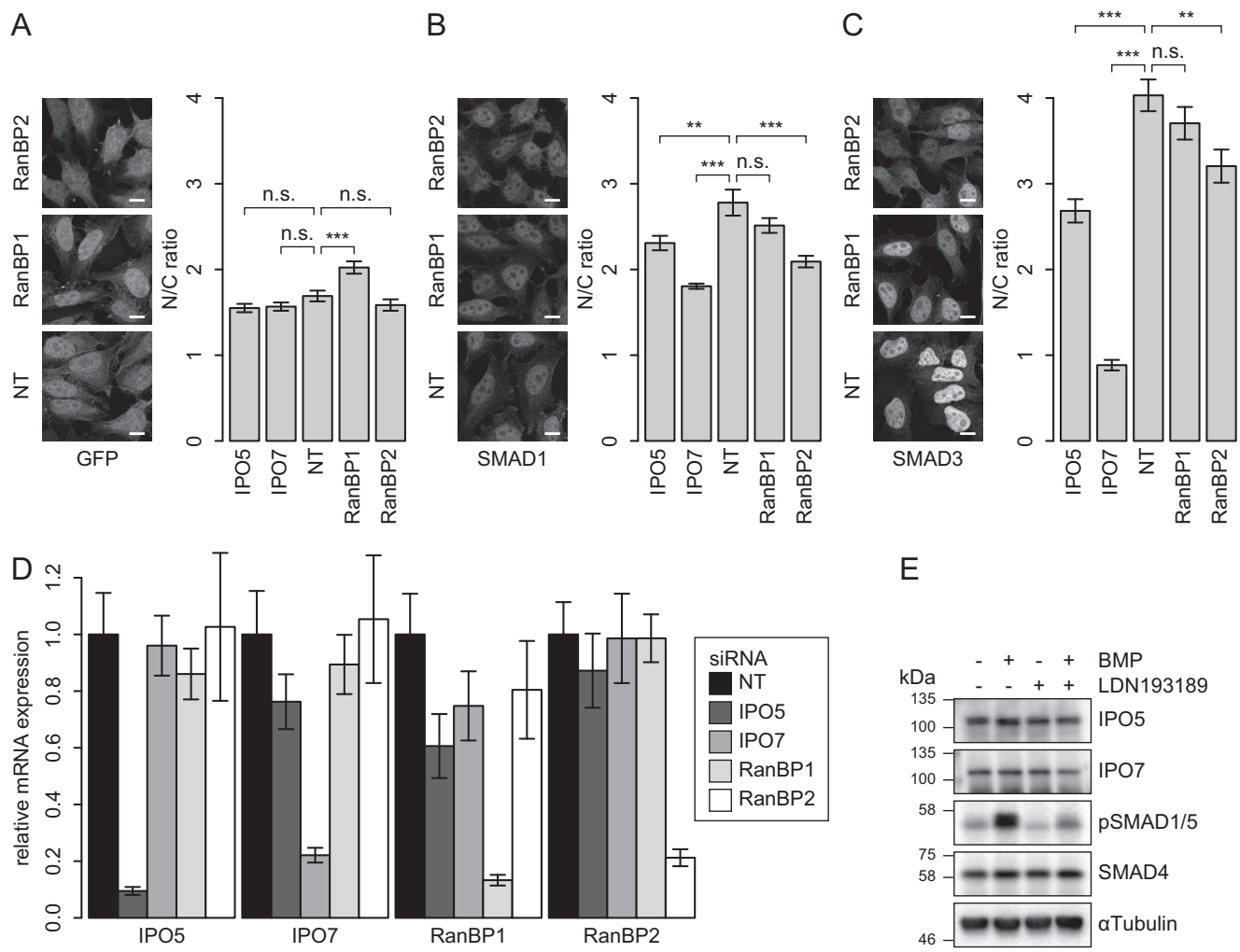

FIGURE 9. **Knockdown of RanBP2 but not RanBP1 reduces nuclear localization of SMAD1 and -3.** *A–C,* HeLa cell lines were transfected with siRNA against non-targeting, IPO5, IPO7, RanBP1, or RanBP2. Cells were induced with 1 μg/ml of doxycycline for 16 h prior to fixing and analyzed 72 h after siRNA transfection using confocal microscopy. Nuclear and cytoplasmic GFP intensities were quantified using ImageJ. *Bars* represent average N/C ratio, *error bars* represent mean ± S.E. Significant differences are indicated for various significance levels (***, $p < 0.001$; **, $0.001 < p < 0.01$; *, $0.01 < p < 0.05$; *n.s.*, not significant). *Scale bar*, 10 μm. *A,* GFP N/C ratios. Technical replication $n = 50$, 48, 44, 49, and 40. *B,* SMAD1 N/C ratios. Technical replication $n = 45$, 63, 43, 55, and 56. *C,* SMAD3 N/C ratios. Technical replication $n = 52$, 39, 59, 37, and 49. *D,* knockdown efficiency of non-targeting, IPO5, IPO7, RanBP1, and RanBP2 in non-induced HeLa GFP cells. Cells were reverse transfected with siNT, siIPO5, siIPO7, siRanBP1, or siRanBP2 and collected after 72 h. Samples were analyzed using qRT-PCR. *Bars* represent average expression corrected for ACTIN and normalized to the siNT control. *Error bars* represent mean ± S.D. Technical replication $n = 3$ for all samples. *E,* IPO5 and IPO7 levels do not change upon BMP stimulation. U-2 OS cells were treated with 100 nM LDN193189 inhibitor for 24 h and subsequently stimulated with 10 ng/ml BMP for 6 h as indicated. Immunoblot was probed using IPO5, IPO7, pSMAD1/5, SMAD4 and Tubulin antibodies.

residues required for R-SMAD phosphorylation and protein activation (6–8). This resulted in fusion constructs that could be phosphorylated upon stimulation of their receptors using their respective ligands (Fig. 3). However, the possibility still remains that interaction partners have been missed due to N-terminal tagging of SMAD proteins. In our experiments we confirmed binding of the transcriptional repressor LEMD3 to SMAD3 in the nucleus and provide evidence that LEMD3 and SMAD4 binding are mutually exclusive (Fig. 5). Interestingly, no LEMD3 binding to other R-SMADs is observed, whereas SKI and SKIL are identified in SMAD2/3 and -4, which indicates a high specificity in repressor interactions.

Activated SMAD proteins stimulate gene transcription, but the exact nature of their nuclear coactivators has not been determined in much detail. We provide evidence that Mediator, TFIID, and SET/MLL but not BAF complex could participate in transcription activation by the SMAD1 and SMAD2 proteins. The observation of specific co-activators for specific SMAD family members warrants a further study into the downstream transcription activation pathways for TGF-β and BMP signaling.

Experimental Procedures

Plasmids—PCR was performed on plasmids containing SMAD cDNAs using primers containing attB1 or attB2 sites to obtain Gateway compatible constructs (Table 1) (34). FLAG-SMAD2 and FLAG-SMAD4 cDNAs (35) were generous gifts from Dr. Peter ten Dijke (Leiden University, Leiden, The Netherlands). IMAGE clones 3546771, 6094328, 3906006, 3632931, 30915321, and 8143763 were purchased for SMAD1, -3, -5, -6, -7, and -9, respectively, from Dharmacon (Lafayette, CO). PCR products were recombined with pDON201 in a Gateway BP reaction to obtain pENTR vectors according to the manufacturer's instructions (Thermo Fischer Scientific, Waltham, MA). All pENTR vectors were confirmed using Sanger sequencing.

Sequencing showed SMAD1 to be a V140L variant compared with the refseq sequence. All other SMADs were identical to the refseq. To obtain HeLa FRT compatible expression vectors pENTR vectors containing SMAD variants were recombined with Gateway-compatible pCDNA5/FRT/TO/N-GFP in an LR reaction according to the manufacturer's instructions (Thermo Fischer Scientific, Waltham, MA). SMAD3 mutagenesis PCR was performed using mutagenesis primers in Table 1. pCDNA3.1-FLAG-IPO5 (36) was a generous gift from Dr. Yi-Shuian Huang (Institute of Biomedical Sciences, Taipei, Taiwan). pME18S-FLAG-hIPO7 (pTIB435) (37) was a generous gift from Dr. Tohru Itoh (The University of Tokyo, Tokyo, Japan).

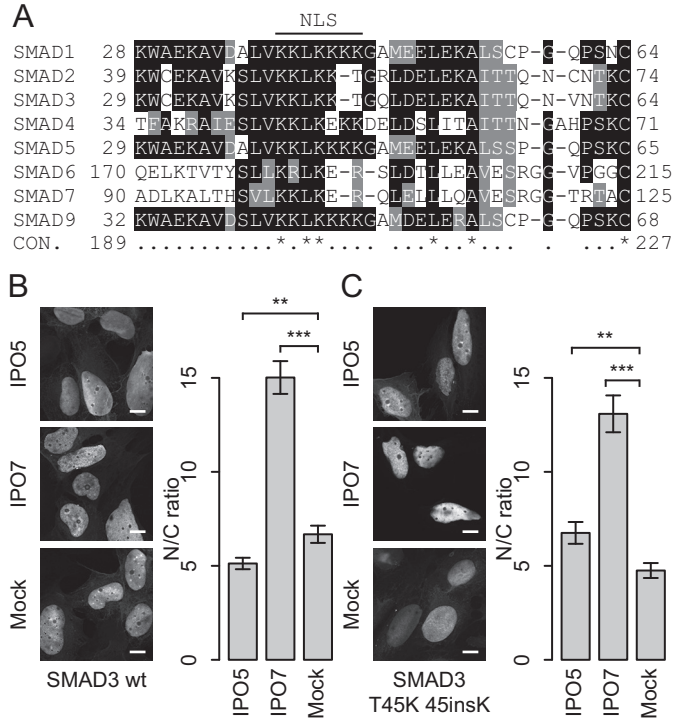

FIGURE 10. **Extension of the SMAD3 NLS allows for IPO5-mediated nuclear localization.** *A,* multiple sequence alignment for the SMADs. Clustering was performed using Clustal Omega. NLS sequence is indicated *above*. *Con*., consensus. *B* and *C,* U-2 OS cells were seeded on coverslips and transfected using a combination of GFP-SMAD3 wt or T45K 45insK with FLAG-IPO5, FLAG-IPO7, or mock. Cells were fixed 48 h after transfection and analyzed using confocal microscopy. Nuclear and cytoplasmic intensities were quantified using ImageJ. Shown is the combined data of $n = 2$ biological replicates with varying technical replication *n* specified per set. *Bars* represent average N/C ratio, *error bars* represent mean ± S.E. Significant differences are indicated for various significance levels (***, $p < 0.001$; **, $0.001 < p < 0.01$; *, $0.01 < p < 0.05$; *n.s.*, not significant). *Scale bar*, 10 μm. *B,* SMAD3 wt N/C ratios. Technical replication $n = 66$, 97, and 82. *C,* SMAD3 T45K 45insK N/C ratios. Technical replication $n = 70$, 92, and 82.

Cell Culture—HeLa cells containing the Flp recombination target (FRT) site and Tet repressor were grown in Dulbecco's modified Eagle's medium (DMEM) containing 4.5 g/liter of glucose supplemented with 10% (v/v) fetal bovine serum, 10 mM L-glutamine, 100 units/ml of penicillin, and 100 units/ml of streptomycin. HeLa FRT parental cell line growth medium was supplemented with 5 μg/ml of blasticidin S (InvivoGen, San Diego, CA) and 200 μg/ml of zeocin (Invitrogen) to select for the FRT site and Tet repressor. To generate cell lines containing stable integration of GFP-tagged proteins, cells were seeded in culture medium without blasticidin S and zeocin antibiotics 8 h prior to transfection. Stable doxycycline-inducible HeLa cell lines were created by co-transfecting the pOG44 Flp recombinase expression vector along with pCDNA5/FRT/TO expression vectors into HeLa FRT cells using polyethyleneimine (PEI). 48 h after transfection growth medium was supplemented with 250 μg/ml of hygromycin B (Roche Diagnostics, Mannheim, Germany) and 5 μg/ml of blasticidin S to select for expression vector integration and Tet repressor.

Immunoblot Analysis—Cells were seeded in 6-well plates at a density of 30,000 cells/well. Cells were induced 16 to 20 h prior to harvesting by addition of 1 μg/ml of doxycycline to the culture media unless otherwise stated. Stimulation with TGF-β_1 (number 8915LC, Cell Signaling) or rhBMP-2 (355-BEC, R&D systems, Minneapolis, MN) and inhibition with SB431542 (number 616461, Calbiochem) or LDN193189 (SML0559, Sigma) was performed by addition of the listed concentrations and duration prior to harvesting. Cells were lysed in sample buffer (160 mM Tris-HCl, pH 6.8, 4% SDS, 20% glycerol, 0.05% bromphenol blue) and equal amounts of protein were run on a 10% SDS-PAGE and transferred onto PVDF membrane. The membrane was developed with the appropriate antibodies and ECL and scanned using ImageQuant LAS 4000.

TABLE 1
Primers used for cloning

Primer	Sequence
SMAD1 FW	GGGG ACA AGT TTG TAC AAA AAA GCA GGC TTC AAT GTG ACA AGT TTA TTT TCC TTT AC
SMAD2 FW	GGGG ACA AGT TTG TAC AAA AAA GCA GGC TTC TCG TCC ATC TTG CCA TTC AC
SMAD3 FW	GGGG ACA AGT TTG TAC AAA AAA GCA GGC TTC TCG TCC ATC CTG CCT TTC AC
SMAD4 FW	GGGG ACA AGT TTG TAC AAA AAA GCA GGC TTC GAC AAT ATG TCT ATT ACG AAT AC
SMAD5 FW	GGGG ACA AGT TTG TAC AAA AAA GCA GGC TTC ACG TCA ATG GCC AGC TTG
SMAD6 FW	GGGG ACA AGT TTG TAC AAA AAA GCA GGC TTC TTC AGG TCC AAA CGC TCG
SMAD7 FW	GGGG ACA AGT TTG TAC AAA AAA GCA GGC TTC TTC AGG ACC AAA CGA TCT GC
SMAD9 FW	AA AAA GCA GGC TTC CAC TCC ACC ACC CCC ATC AGC TCC CTC TTC TCC
ADAPT FW	GGGG ACA AGT TTG TAC AAA AAA GCA GGC T
SMAD1 RV	GGGG ACC ACT TTG TAC AAG AAA GCT GGG TC CTA AGA TAC AGA TGA AAT AGG ATT ATG AG
SMAD2 RV	GGGG ACC ACT TTG TAC AAG AAA GCT GGG TC CTA TGA CAT GCT TGA GCA ACG CAC
SMAD3 RV	GGGG ACC ACT TTG TAC AAG AAA GCT GGG TC CTA AGA CAC ACT GGA ACA GCG GAT G
SMAD4 RV	GGGG ACC ACT TTG TAC AAG AAA GCT GGG TC CTA GTC TAA AGG TTG TGG GTC TG
SMAD5 RV	GGGG ACC ACT TTG TAC AAG AAA GCT GGG TC CTA TGA AAC AGA AGA TAT GGG GTT CAG AG
SMAD6 RV	GGGG ACC ACT TTG TAC AAG AAA GCT GGG TC CTA TCT GGG GTT GTT GAG GAG G
SMAD7 RV	GGGG ACC ACT TTG TAC AAG AAA GCT GGG TC CTA CCG GCT GTT GAA GAT GAC C
SMAD9 Rv	AG AAA GCT GGG TC CTA AGA CAC TGA AGA AAT GGG GTT ATG TGG AGA GCC
ADAPT RV	GGGG ACC ACT TTG TAC AAG AAA GCT GGG T
SMAD3 T45K 45INSK FW	GGT CAA GAA ACT CAA GAA GAA GAA AGG GCA GCT GGA CGA GCT GG
SMAD3 T45K 45INSK RV	CCA GCT CGT CCA GCT GCC CTT TCT TCT TCT TGA GTT TCT TGA CC

Antibodies—Antibodies were used from the following sources: GAPDH (clone 6C5, mAb374, Millipore), GFP (gift from Geert Kops), IPO5 (H-4, sc-17802, Santa Cruz), IPO7 (ab99273, Abcam), phospho-SMAD1/5 (D5B10, number 11971, Cell Signaling), phospho-SMAD2 (138D4, number 3108, Cell Signaling), SMAD2/3 (N-19, sc-6032, Santa Cruz), SMAD4 (number 9515, Cell Signaling), TBP (20C7 in-house hybridoma (38)), α-Tubulin (DM1A, CP06, Calbiochem).

Nuclear Extract Preparation and GFP Affinity Purification—Cytoplasmic and nuclear extracts were prepared as described (39) with the exception that DTT was omitted from buffer C. Protein concentration was determined using Bradford assay as described before (39). GFP affinity purification was essentially performed as described (39) with buffer C lacking DTT. Sample binding was performed for 30 min on a rotating wheel at 4 °C using 1 mg of input protein. Peptides were eluted from the beads by a 2-h trypsin incubation in elution buffer (100 mM Tris-HCl, pH 7.5, 2 M urea, 10 mM DTT). Eluate was collected and beads were eluted for a second time. Eluates were combined and trypsin digested overnight. Tryptic digests were desalted using Stage-tips (40).

Mass Spectrometry—Tryptic peptides were separated using an EASY-nLC 1000 (Thermo Fischer Scientific) mounted with a C18 column operating online with an LTQ Orbitrap Velos. An acetonitrile gradient (0–80%) was applied over 2 h to elute peptides from the column. Peptides were ionized using ESI. The top 15 most abundant peptides were selected for fragmentation using CID for MS/MS. Proteins were identified from the raw data using MaxQuant version 1.5.2.8 using the Uniprot human FASTA database. Perseus version 1.5.1.6 was used to filter for contaminants and reverse hits. LFQ values were log2 transformed and groups based on cell line, extract type, and bead type were defined. A filter was applied to remove contaminants and proteins that could be identified using a reversed database, which are very likely false-positive identifications. Then a filter was applied that identified proteins that were present at least 3 of 3 times within at least one combination of conditions (bead type, extract and cell line) resulting in a total of 3649 selected proteins after Perseus filtering. The median of each group was taken and data were plotted using R version 3.2.2 (41) with Rstudio version 0.99.486.

siRNA Transfection—Cells were transfected in a reverse transfection protocol using Hiperfect (Qiagen, Valencia, CA) according to the manufacturer's instructions. In short, 50 μl of a SMARTpool of four siRNAs (25 nM each) was dispensed in a 12-well plate (Costar, 3513, Corning, New York, NY) containing 15-mm diameter coverglasses (Paul Marienfeld GmbH & Co. KG, Lauda Königshofen, Germany). Transfection mixture (4 μl of Hiperfect in total volume of 150 μl of Opti-MEM (Invitrogen) per well) was added followed by a 30-min incubation at room temperature. Meanwhile, cells were counted and 30,000 cells/well were added in 800 μl. Cells were fixed 72 h after transfection.

Transient Transfection—U-2 OS osteosarcoma cells were counted and seeded in 30,000 cells/well in a 12-well plate containing 15-mm diameter coverglasses. Cells were left overnight to attach and expression vectors were transfected using PEI. Cells were fixed 48 h after transfection.

TABLE 2
Primers used for qRT-PCR

Primer	Sequence
ACTIN FW	AGAAAATCTGGCACCACACC
ACTIN RV	AGAGGCGTACAGGGATAGCA
IPO5 FW	TGCTCTAGATCGAATGGCTTG
IPO5 RV	ATGCCGGTATTTCCAGTCAG
IPO7 FW	GTGAACAGGGATGTACCTAATGAA
IPO7 RV	ATGTAAGGCCCACTTCTTGC
RANBP1 FW	CCAATAGTTTCTCTTCCTGAGCA
RANBP1 RV	GAGGCAAATCGGAACAGTTT
RANBP2 FW	TGTAGTGATACTGATGAAGACAATGG
RANBP2 RV	TTGTGCTAGTTATTTCTTCTGTCTGAG

Microscopy Slide Preparation—Coverglasses containing treated cells were washed once with phosphate-buffered saline (PBS). Cells were fixed by incubation with 4% formaldehyde in PBS for 20 min at room temperature. Cells were incubated with DAPI solution (2 mg/liter of 4′,6-diamidino-2-phenylindole (Sigma) in 50 mM Tris-HCl, pH 7.4, 100 mM NaCl) to stain nuclei. Coverglasses were mounted onto microscope slides (Thermo Fischer Scientific) using Immu-Mount (Invitrogen) and left to dry overnight at 4 °C.

Confocal Microscopy—Images were taken using a Zeiss LSM 510 META confocal microscope with PLAN Apochromat Oil-DIC ×63/1.4 objective. Samples were scanned using a 405-nm Violet Diode Laser for DAPI staining and a 488-nm argon laser for GFP. Microscope gain and offset settings were kept constant within experiments that compared a fusion protein in different conditions. Nuclear and cytoplasmic intensities were measured using ImageJ version 1.50d. Plots and statistics were generated using R version 3.2.1 with Rstudio version 0.99.473.

Expression Analysis Quantitative (q)RT-PCR—Total RNA was isolated from siRNA-treated cells 72 h after transfection using RNeasy kit (Qiagen) including a DNase treatment using RNase-free DNase set (Qiagen) according to the manufacturer's instructions. 500 ng of total RNA was used for cDNA synthesis (Superscript II, Invitrogen) using random primers. A 25-μl qRT-PCR was performed in a CFX Connect Real-time PCR Detection System (Bio-Rad) using iQ SYBR Green Supermix (Bio-Rad). Primers used for qRT-PCR can be found in Table 2.

Author Contributions—R. B. and A. S. performed cloning and mass spectrometry experiments. R. B. performed immunofluorescence experiments and analysis of the mass spectrometry data. H. v. T. provided technical assistance and contributed to the immunoblots. H. V. and R. v. E. performed technical assistance for the mass spectrometry experiments. M. T. coordinated the study. R. B. wrote the paper, which was corrected by M. T. and reviewed by all authors.

Acknowledgments—We thank Proteins at Work (www.netherlands proteomicscenter.nl/paw) for providing usage and support of their mass spectrometry facility. The mass spectrometry proteomics data have been deposited to the ProteomeXchange Consortium via the PRIDE (42) partner repository with the dataset identifier PXD004529. Dr. Peter ten Dijke, Dr. Yi-Shuian Huang, and Dr. Tohru Itoh are thanked for providing plasmids. Furthermore, the authors thank Dr. Simona Capponi and Ana Rita Lourenço, MSc, for critical reading of the manuscript and all the members of the Timmers group for helpful discussions and suggestions.

References

1. Koster, M. J., Snel, B., and Timmers, H. T. (2015) Genesis of chromatin and transcription dynamics in the origin of species. *Cell* **161,** 724–736
2. Vaquerizas, J. M., Kummerfeld, S. K., Teichmann, S. A., and Luscombe, N. M. (2009) A census of human transcription factors: function, expression and evolution. *Nat. Rev. Genet.* **10,** 252–263
3. Kandoth, C., McLellan, M. D., Vandin, F., Ye, K., Niu, B., Lu, C., Xie, M., Zhang, Q., McMichael, J. F., Wyczalkowski, M. A., Leiserson, M. D., Miller, C. A., Welch, J. S., Walter, M. J., Wendl, M. C., *et al.* (2013) Mutational landscape and significance across 12 major cancer types. *Nature* **502,** 333–339
4. Lawrence, M. S., Stojanov, P., Mermel, C. H., Robinson, J. T., Garraway, L. A., Golub, T. R., Meyerson, M., Gabriel, S. B., Lander, E. S., and Getz, G. (2014) Discovery and saturation analysis of cancer genes across 21 tumour types. *Nature* **505,** 495–501
5. Ojesina, A. I., Lichtenstein, L., Freeman, S. S., Pedamallu, C. S., Imaz-Rosshandler, I., Pugh, T. J., Cherniack, A. D., Ambrogio, L., Cibulskis, K., Bertelsen, B., Romero-Cordoba, S., Treviño, V., Vazquez-Santillan, K., Guadarrama, A. S., Wright, A. A., *et al.* (2014) Landscape of genomic alterations in cervical carcinomas. *Nature* **506,** 371–375
6. Lechleider, R. J., de Caestecker, M. P., Dehejia, A., Polymeropoulos, M. H., and Roberts, A. B. (1996) Serine phosphorylation, chromosomal localization, and transforming growth factor-β signal transduction by human bsp-1. *J. Biol. Chem.* **271,** 17617–17620
7. Yingling, J. M., Das, P., Savage, C., Zhang, M., Padgett, R. W., and Wang, X. F. (1996) Mammalian dwarfins are phosphorylated in response to transforming growth factor β and are implicated in control of cell growth. *Proc. Natl. Acad. Sci. U.S.A.* **93,** 8940–8944
8. Zhang, Y., Feng, X., We, R., and Derynck, R. (1996) Receptor-associated Mad homologues synergize as effectors of the TGF-beta response. *Nature* **383,** 168–172
9. Xiao, Z., Latek, R., and Lodish, H. F. (2003) An extended bipartite nuclear localization signal in Smad4 is required for its nuclear import and transcriptional activity. *Oncogene* **22,** 1057–1069
10. Chen, X., and Xu, L. (2010) Specific nucleoporin requirement for Smad nuclear translocation. *Mol. Cell Biol.* **30,** 4022–4034
11. Xu, L., Yao, X., Chen, X., Lu, P., Zhang, B., and Ip, Y. T. (2007) Msk is required for nuclear import of TGF-β/BMP-activated Smads. *J. Cell Biol.* **178,** 981–994
12. Xiao, Z., Liu, X., Henis, Y. I., and Lodish, H. F. (2000) A distinct nuclear localization signal in the N terminus of Smad 3 determines its ligand-induced nuclear translocation. *Proc. Natl. Acad. Sci. U.S.A.* **97,** 7853–7858
13. Xiao, Z., Watson, N., Rodriguez, C., and Lodish, H. F. (2001) Nucleocytoplasmic shuttling of Smad1 conferred by its nuclear localization and nuclear export signals. *J. Biol. Chem.* **276,** 39404–39410
14. Tsubakihara, Y., Hikita, A., Yamamoto, S., Matsushita, S., Matsushita, N., Oshima, Y., Miyazawa, K., and Imamura, T. (2015) Arkadia enhances BMP signalling through ubiquitylation and degradation of Smad6. *J. Biochem.* **158,** 61–71
15. Lebrun, J. J., Takabe, K., Chen, Y., and Vale, W. (1999) Roles of pathway-specific and inhibitory Smads in activin receptor signaling. *Mol. Endocrinol.* **13,** 15–23
16. Kavsak, P., Rasmussen, R. K., Causing, C. G., Bonni, S., Zhu, H., Thomsen, G. H., and Wrana, J. L. (2000) Smad7 binds to Smurf2 to form an E3 ubiquitin ligase that targets the TGF β receptor for degradation. *Mol. Cell* **6,** 1365–1375
17. Hata, A., Lagna, G., Massagué, J., and Hemmati-Brivanlou, A. (1998) Smad6 inhibits BMP/Smad1 signaling by specifically competing with the Smad4 tumor suppressor. *Genes Dev.* **12,** 186–197
18. Hjelmeland, M. D., Hjelmeland, A. B., Sathornsumetee, S., Reese, E. D., Herbstreith, M. H., Laping, N. J., Friedman, H. S., Bigner, D. D., Wang, X. F., and Rich, J. N. (2004) SB-431542, a small molecule transforming growth factor-β-receptor antagonist, inhibits human glioma cell line proliferation and motility. *Mol. Cancer Ther.* **3,** 737–745
19. Levy, L., Howell, M., Das, D., Harkin, S., Episkopou, V., and Hill, C. S. (2007) Arkadia activates Smad3/Smad4-dependent transcription by triggering signal-induced SnoN degradation. *Mol. Cell Biol.* **27,** 6068–6083
20. Takahata, M., Inoue, Y., Tsuda, H., Imoto, I., Koinuma, D., Hayashi, M., Ichikura, T., Yamori, T., Nagasaki, K., Yoshida, M., Matsuoka, M., Morishita, K., Yuki, K., Hanyu, A., Miyazawa, K., *et al.* (2009) SKI and MEL1 cooperate to inhibit transforming growth factor-β signal in gastric cancer cells. *J. Biol. Chem.* **284,** 3334–3344
21. Lin, F., Morrison, J. M., Wu, W., and Worman, H. J. (2005) MAN1, an integral protein of the inner nuclear membrane, binds Smad2 and Smad3 and antagonizes transforming growth factor-β signaling. *Hum. Mol. Genet.* **14,** 437–445
22. Pan, D., Estévez-Salmerón, L. D., Stroschein, S. L., Zhu, X., He, J., Zhou, S., and Luo, K. (2005) The integral inner nuclear membrane protein MAN1 physically interacts with the R-Smad proteins to repress signaling by the transforming growth factor-β superfamily of cytokines. *J. Biol. Chem.* **280,** 15992–16001
23. Yaseen, N. R., and Blobel, G. (1997) Cloning and characterization of human karyopherin β3. *Proc. Natl. Acad. Sci. U.S.A.* **94,** 4451–4456
24. Deane, R., Schäfer, W., Zimmermann, H. P., Mueller, L., Görlich, D., Prehn, S., Ponstingl, H., and Bischoff, F. R. (1997) Ran-binding protein 5 (RanBP5) is related to the nuclear transport factor importin-β but interacts differently with RanBP1. *Mol. Cell Biol.* **17,** 5087–5096
25. Varelas, X., Sakuma, R., Samavarchi-Tehrani, P., Peerani, R., Rao, B. M., Dembowy, J., Yaffe, M. B., Zandstra, P. W., and Wrana, J. L. (2008) TAZ controls Smad nucleocytoplasmic shuttling and regulates human embryonic stem-cell self-renewal. *Nat. Cell Biol.* **10,** 837–848
26. Xiao, Z., Liu, X., and Lodish, H. F. (2000) Importin β mediates nuclear translocation of Smad 3. *J. Biol. Chem.* **275,** 23425–23428
27. Xu, J., Wang, A. H., Oses-Prieto, J., Makhijani, K., Katsuno, Y., Pei, M., Yan, L., Zheng, Y. G., Burlingame, A., Brückner, K., and Derynck, R. (2013) Arginine methylation initiates BMP-induced Smad signaling. *Mol. Cell* **51,** 5–19
28. Guo, X., and Wang, X. F. (2013) A P(E)RM(I)T for BMP signaling. *Mol. Cell* **51,** 1–2
29. Singh, A. M., Reynolds, D., Cliff, T., Ohtsuka, S., Mattheyses, A. L., Sun, Y., Menendez, L., Kulik, M., and Dalton, S. (2012) Signaling network crosstalk in human pluripotent cells: a Smad2/3-regulated switch that controls the balance between self-renewal and differentiation. *Cell Stem Cell* **10,** 312–326
30. Alarcón, C., Zaromytidou, A. I., Xi, Q., Gao, S., Yu, J., Fujisawa, S., Barlas, A., Miller, A. N., Manova-Todorova, K., Macias, M. J., Sapkota, G., Pan, D., and Massagué, J. (2009) Nuclear CDKs drive Smad transcriptional activation and turnover in BMP and TGF-β pathways. *Cell* **139,** 757–769
31. Gao, S., Alarcón, C., Sapkota, G., Rahman, S., Chen, P. Y., Goerner, N., Macias, M. J., Erdjument-Bromage, H., Tempst, P., and Massagué, J. (2009) Ubiquitin ligase Nedd4L targets activated Smad2/3 to limit TGF-β signaling. *Mol. Cell* **36,** 457–468
32. Isogaya, K., Koinuma, D., Tsutsumi, S., Saito, R. A., Miyazawa, K., Aburatani, H., and Miyazono, K. (2014) A Smad3 and TTF-1/NKX2–1 complex regulates Smad4-independent gene expression. *Cell Res.* **24,** 994–1008
33. Katagiri, T., and Watabe, T. (2016) Bone morphogenetic proteins. *Cold Spring Harbor Perspect. Biol.* **8,** 10.1101/cshperspect.a021899
34. Hartley, J. L., Temple, G. F., and Brasch, M. A. (2000) DNA cloning using *in vitro* site-specific recombination. *Genome Res.* **10,** 1788–1795
35. Nakao, A., Imamura, T., Souchelnytskyi, S., Kawabata, M., Ishisaki, A., Oeda, E., Tamaki, K., Hanai, J., Heldin, C. H., Miyazono, K., and ten Dijke, P. (1997) TGF-β receptor-mediated signalling through Smad2, Smad3 and Smad4. *EMBO J.* **16,** 5353–5362
36. Chao, H. W., Lai, Y. T., Lu, Y. L., Lin, C. L., Mai, W., and Huang, Y. S. (2012) NMDAR signaling facilitates the IPO5-mediated nuclear import of CPEB3. *Nucleic Acids Res.* **40,** 8484–8498
37. Saijou, E., Itoh, T., Kim, K. W., Iemura, S., Natsume, T., and Miyajima, A. (2007) Nucleocytoplasmic shuttling of the zinc finger protein EZI Is mediated by importin-7-dependent nuclear import and CRM1-independent export mechanisms. *J. Biol. Chem.* **282,** 32327–32337
38. Pereira, L. A., van der Knaap, J. A., van den Boom, V., van den Heuvel, F. A., and Timmers, H. T. (2001) TAF(II)170 interacts with the concave surface of TATA-binding protein to inhibit its DNA binding activity. *Mol. Cell Biol.* **21,** 7523–7534

39. Baymaz, H. I., Spruijt, C. G., and Vermeulen, M. (2014) Identifying nuclear protein-protein interactions using GFP affinity purification and SILAC-based quantitative mass spectrometry. *Methods Mol. Biol.* **1188,** 207–226
40. Rappsilber, J., Ishihama, Y., and Mann, M. (2003) Stop and go extraction tips for matrix-assisted laser desorption/ionization, nanoelectrospray, and LC/MS sample pretreatment in proteomics. *Anal. Chem.* **75,** 663–670
41. R Core Team (2015) R: a language and environment for statistical computing. R Foundation for Statistical Computing, Vienna, Austria
42. Vizcaíno, J. A., Csordas, A., del-Toro, N., Dianes, J. A., Griss, J., Lavidas, I., Mayer, G., Perez-Riverol, Y., Reisinger, F., Ternent, T., Xu, Q. W., Wang, R., and Hermjakob, H. (2016) 2016 update of the PRIDE database and its related tools. *Nucleic Acids Res.* **44,** D447–456